Broadband alignment scheme for a stepper system using combinations of diffractive and refractive lenses

Yasuhiro Yoshitake and G. Michael Morris

By using broadband illumination, a stepper alignment system is less sensitive to asymmetric coverage of photoresist around alignment targets and realizes high accuracy. However, a projection lens causes chromatic aberrations at the wavelengths in the broadband light. To correct the chromatic aberrations, we employed a Schupmann system composed of a projection lens, an achromat lens, and a refractive–diffractive hybrid lens. With the proposed system the spread of image planes and the magnification difference in the spectral range from 550 to 650 nm can be reduced to 50 μm and 0.05%, whereas without the correction system these values are 11.28 mm and 1.18%, respectively.

1. Introduction

An exposure apparatus known as a stepper is a main production machine for semiconductor fabrication. A stepper is used to image circuit patterns recorded on a mask and to print them on a wafer through the use of a step-and-repeat procedure. Generally, the circuit patterns are stratified into many layers. To retain large-scale integrated circuit performance, one must accurately align a given layer to the top layer on the wafer. Alignment is usually accomplished by the detection of alignment marks on the wafer. Prior to exposure, the wafer is usually coated with a photoresist-type material through the use of a spin-coating method. In the coating process, the photoresist spreads in the radial directions and often forms an asymmetrical shape around the alignment marks. The intensity of light reflected from the photoresist is sensitive to the thickness of the photoresist. Therefore, images of the asymmetrically covered alignment marks can be deformed asymmetrically; this produces degradation in the alignment accuracy. However, it is well known that broadband illumination can reduce this problem.[1] With broadband illumination, the intensity of the reflected light is less sensitive to fluctuation of the photoresist thickness, and symmetrical images can be expected in spite of asymmetrical photoresist coverage.

A broadband-light alignment system that is separated from the projection lens, i.e., a system that is not through the lens (TTL), was described by Nishi.[2] However, there are difficulties with Nishi's system. In practice, the alignment system is mounted with structures of steel, and the system can move slightly as a result of environmental factors, such as temperature or vibration. For instance, if the alignment system moves by 0.05 μm, a non-TTL system will have an alignment error of 0.05 μm. However, a TTL system can reduce the error corresponding to the reduction ratio of the projection lens. Typically the reduction ratio is 1/5. Therefore, even if the alignment system moves by 0.05 μm, a TTL system will have only a 0.01-μm error. There is, however, a different problem with a TTL alignment system that uses broadband light. Normally the projection lens is designed to have the best performance at the exposure wavelength (typically, an ultraviolet wavelength). The wavelength of the light used for alignment should be selected at a different wavelength from the exposure light so as not to expose the photoresist. Therefore, TTL systems that use broadband light have difficulty generating high-quality images because of the longitudinal chromatic aberration introduced by the projection lens.

To overcome this problem, Komoriya *et al.*[3] described a chromatic aberration correction system. However, to counteract the dispersion introduced by the projection lens, this invention had to employ

Y. Yoshitake is with the Production Engineering Research Laboratory, Hitachi, Ltd., 292 Yoshida-cho, Totsuka-ku, Yokohama 244, Japan. G. M. Morris is with the Institute of Optics, University of Rochester, Rochester, New York, 14627.

Received 23 September 1993; revised manuscript received 28 March 1994.

0003-6935/94/347971-09$06.00/0.

many lens elements. The projection lens itself usually consists of more than ten elements, and each glass element introduces dispersion, which causes chromatic aberration. Therefore, using a conventional approach to correct these aberrations, one essentially needs to use a comparable number of lenses in the alignment system. To reduce the number of elements, the lens elements in the correction system must provide a large and negative value for the dispersion. Glass elements cannot satisfy this requirement. However, a diffractive lens has precisely these characteristics. The dispersion (or Abbe V number) of a diffractive lens is -3.45, whereas that of glass remains between 20 and 80.[4] The V number of a diffractive lens is approximately seven times more dispersive than that of any known glass and exhibits a negative dispersion, i.e., with a diffractive lens a red ray of light bends more than a blue one, whereas with glass a blue ray bends more than a red one. The operation of a diffractive lens relies on interference and diffraction, rather than on the refraction of light as in a glass lens. Through the utilization of a diffractive lens, it is possible to reduce significantly the number of elements necessary for the correction system.

In this paper we consider a broadband alignment scheme designed for operation with an h-line (405.5-nm) projection lens. In Section 2 the specifications of the alignment system are given. In Section 3 a solution for an achromatic alignment system is illustrated, and the system is optimized with a commercial lens design program. The fabrication method for the diffractive–refractive lenses is discussed in Section 4, and experimental results are given.

2. Specification of the Alignment System

For a projection lens, we selected an h-line (405.5-nm) lens from the patent literature[5] and modified it to improve the optical performance at the h-line wavelength. The modified lens has a reduction ratio of 1/5, a N.A. of 0.35, and a field size of 10 mm × 10 mm. To evaluate the effect of broadband illumination, we examined a simple structure composed of photoresist and a silicon substrate as shown in Fig. 1. Thin-film theory can be used to predict the relation between the reflected intensity and photoresist thickness.[6] According to this theory, one obtains the reflected intensity at a given thickness, d, by using the following formula:

$$I(d) = \tfrac{1}{2}[|R_p(d)|^2 + |R_s(d)|^2], \tag{1}$$

in which

$$|R_k(d)|^2 = \int_{\lambda_A}^{\lambda_B}\int_0^{\theta_{\max}} \frac{r_{k,1}(\theta_1)^2 + r_{k,2}(\theta_1)^2 + 2r_{k,1}(\theta_1)r_{k,2}(\theta_1)\cos\,\delta(d,\theta_1,\lambda)}{1 + r_{k,1}(\theta_1)^2 r_{k,2}(\theta_1)^2 + 2r_{k,1}(\theta_1)r_{k,2}(\theta_1)\cos\,\delta(d,\theta_1,\lambda)}\,d\theta_1 d\lambda \quad (k = p, s),$$

$$\delta(d,\theta_1,\lambda) = \frac{2\pi}{\lambda}\,2n_2 d\left(1 - \frac{\sin^2\theta_1}{{n_2}^2}\right)^{1/2},$$

$$\theta_{\max} = \sin^{-1}\text{N.A.},$$

$$r_{p,i} = \frac{\cos\theta_i/n_i - \cos\theta_{i+1}/n_{i+1}}{\cos\theta_i/n_i + \cos\theta_{i+1}/n_{i+1}} \quad (i = 1, 2),\ p\text{-polarized case},$$

$$r_{s,i} = \frac{n_i\cos\theta_i - n_{i+1}\cos\theta_{i+1}}{n_i\cos\theta_i + n_{i+1}\cos\theta_{i+1}} \quad (i = 1, 2),\ s\text{-polarized case},$$

where the subscripts 1, 2, and 3 indicate air, photoresist, and silicon, respectively, and λ_A and λ_B are the minimum and the maximum wavelengths in the broadband region. The cases of monochromatic illumination (550 nm) and broadband illumination (550–650 nm) are illustrated in Fig. 2. In the broadband illumination case the fluctuations of the reflected intensity, which indicates the sensitivity of the alignment accuracy to the fluctuation of photoresist thickness, smooth rapidly for photoresist thicknesses above 1 μm, whereas in the monochromatic (550-nm) illumination case the fluctuations are still significant for photoresist thicknesses up to 4 μm. In Section 3 we consider the design of an achromatic alignment system that uses broadband light in the spectral range from 550 to 650 nm for illumination.

3. Solution for an Achromatic Alignment System

A solution of an achromatic imaging system that uses diffractive lenses, consisting of a modified Schup-

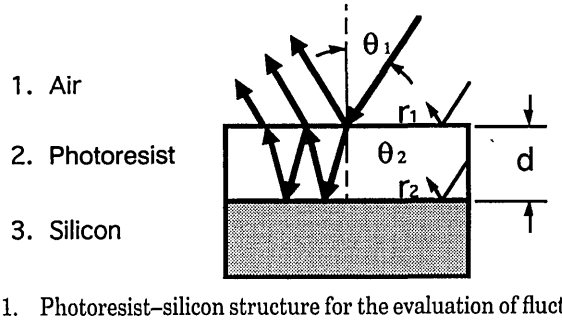

Fig. 1. Photoresist–silicon structure for the evaluation of fluctuation amplitude of reflection intensity.

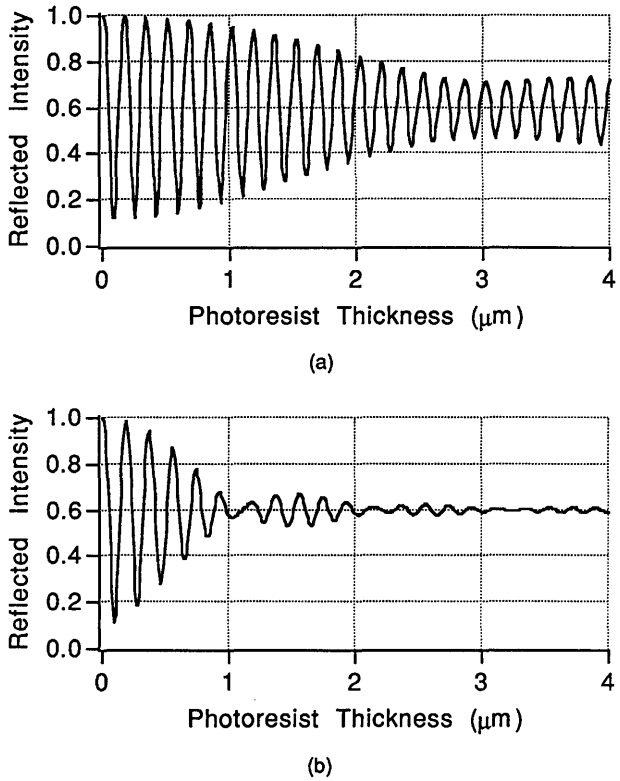

Fig. 2. Reflected intensity versus photoresist thickness in the case of (a) monochromatic illumination and (b) broadband illumination. In (b), the fluctuation amplitude of the reflection intensity converges rapidly near 1 μm; in (a), fluctuation lasts until 4 μm.

mann system,[7] was given by Faklis and Morris.[8] Figure 3 shows a configuration of the Schupmann system. Lens 2 is located at the image point of lens 1 and also images lens 1 onto lens 3. Lens 3 relays the image formed by lens 1. A condition required for achromatic imaging is given by the following equation:

$$\varphi_3(\lambda) = -\frac{B^2}{C^2}[\varphi_1(\lambda) - \varphi_1(\lambda_0)] + \varphi_3(\lambda_0), \qquad (2)$$

where λ is an operating wavelength, λ_0 is the center (or design) wavelength in the range of operating wavelengths, φ_1 is the power of lens 1, φ_3 is the power of lens 3, B is the distance between lens 1 and lens 2, and C is the distance between lens 2 and lens 3. Figure 4 shows a practical configuration. Lenses 1, 2, and 3 in Fig. 3 are replaced by the projection lens, the achromat lens, and the refractive–diffractive hybrid lens, respectively.

Alignment marks are usually located at the edge of the field so that the optical path of the alignment system does not interfere with the exposure light. For our alignment system, the object height is selected to be 10 mm, and it follows that the system is an off-axis optical system. With the h-line projection lens, each wavelength produces a different image point. Figure 5(a) shows the difference in image plane location, ΔL, at wavelength λ, relative to the

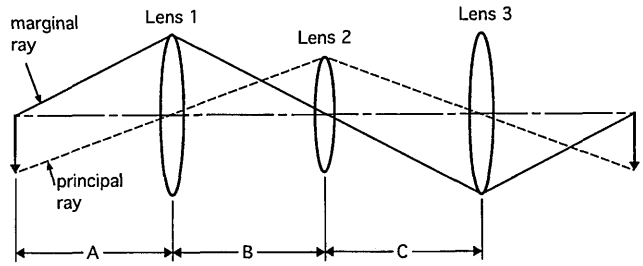

Fig. 3. Layout of a Schupmann lens system. Lens 2 is located at the image point of lens 1 and also images lens 1 onto lens 3. Lens 3 relays the image formed by lens 1.

location of the image plane at the center wavelength (λ_0 = 600 nm), and Fig. 5(b) illustrates the relationship of the image magnification difference, ΔM, at different wavelengths, respectively. It is found that peak-to-peak values of ΔL and ΔM of the h-line projection lens in the spectral range between 550 and 650 nm are 11.28 mm and 1.18%, respectively.

Using thin-lens theory, we find the chromatic change in image height of the principal ray (CCP) of lens 1 in Fig. 2 to be essentially zero. However, the CCP of an actual projection lens is not zero. Figure 6 shows the CCP of the h-line projection lens. The short-dashed curve, the solid curve, and the long-dashed curve indicate the principal rays of wavelengths of 550, 600, and 650 nm, respectively. The CCP denotes the height difference between the rays at wavelengths of 550 and 650 nm at the image plane of light formed with light at the 600-nm wavelength, and it indicates the amount of lateral chromatic aberration.[9] For the achromatic Schupmann system to operate properly, the CCP of the h-line projection lens should be made to be zero. The CCP can be described by the following equation:

$$\mathrm{CCP} = -\frac{1}{u_{k'}}\sum_s n_s\beta_s Y_s \Delta n_s, \qquad (3)$$

in which

$$\Delta n_s = \left(\frac{dn_s}{n_s} - \frac{dn_{s-1}}{n_{s-1}}\right),$$
$$dn_s = n_s(\lambda_2) - n_s(\lambda_1),$$
$$n_s = n_s(\lambda_0),$$

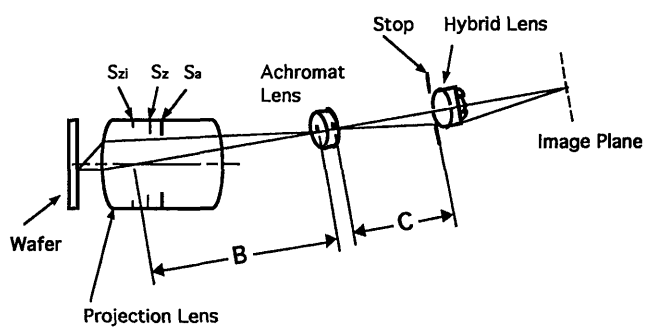

Fig. 4. Practical configuration of an achromatic system based on the Schupmann system. Lenses 1, 2, and 3 in Fig. 3 are replaced by a projection lens, an achromat lens, and a diffractive–refractive hybrid lens, respectively. Symbols S_a, S_z, and S_{zi} are defined in text.

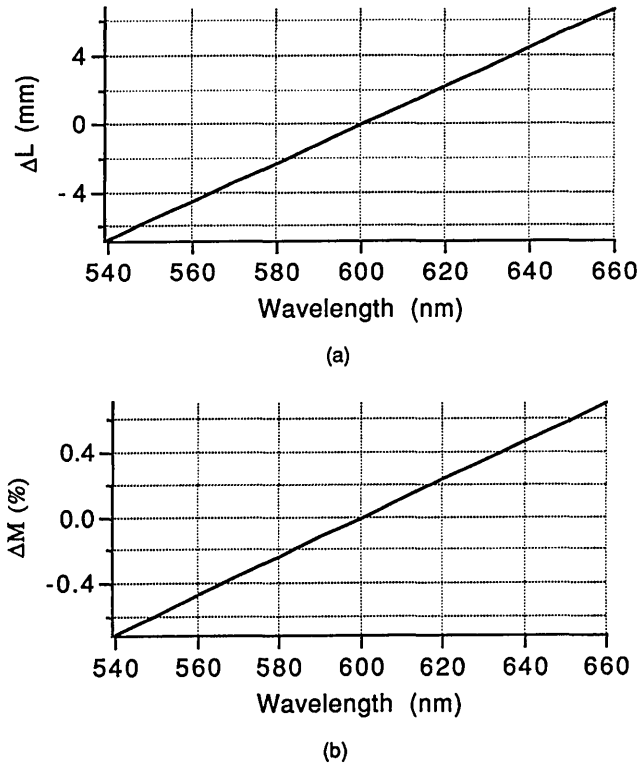

Fig. 5. Chromatic image differences of the h-line projection lens; (a) shows the difference in image plane location, ΔL, at wavelength λ, relative to the location of the image plane at the center wavelength (λ_0 = 600 nm), (b) illustrates the relationship of the image magnification difference, ΔM, at different wavelengths.

where u_k' denotes the convergence angle of the marginal ray in the image space, n_s and β_s are the refractive index and the angle of refraction of the principal ray in the medium after surface S, respectively, and Y_s is the height of the marginal ray.

Figure 7 shows a layout of the h-line projection lens. One can make the CCP be zero by changing the location of the aperture stop. The relation between the aperture stop location and the CCP is shown in Fig. 8. Note that the CCP is zero near surface 15. In fact, when the stop is located 1.9 mm behind surface 14, the CCP becomes exactly zero.

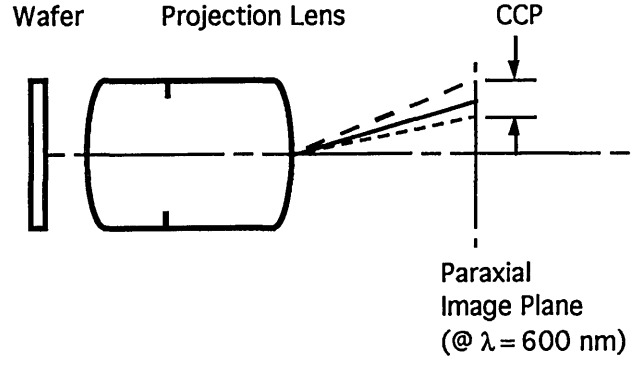

Fig. 6. Illustration of the CCP for the h-line projection lens. The short-dashed curve, the solid curve, the long-dashed curve, and the CCP are defined in text.

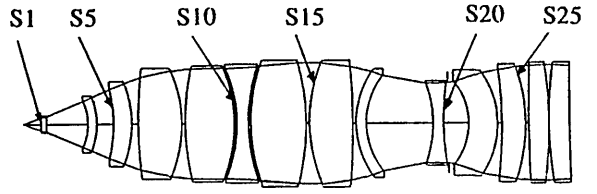

Fig. 7. Layout of the h-line projection lens. The numerals are allotted to the surface in order from the object side.

However, in a practical system it is impossible to set the stop at such a location because it will degrade the performance of the projection lens at the exposure light. Instead, one can obtain the same effect (see Fig. 4) by setting the stop in contact with the refractive–diffractive lens. In Fig. 4 symbol S_a indicates an actual stop of the projection lens. Symbol S_z shows the location of the stop that causes the CCP to be zero, and symbol S_{zi} shows the image of the stop S_z that is seen from the image side. Distance B in Eq. (1) is defined as the distance between the location of S_{zi} and the front principal point of the achromat lens. Distance C is defined as the distance between the rear principal point and the stop of the refractive–diffractive lens. The front principal point of the achromat lens is located at the image point of the projection lens at the center wavelength (λ_0 = 600 nm).

Once a focal length of the achromat lens is determined, one obtains distance C by using the following equation:

$$\frac{1}{F_2} = \frac{1}{B} + \frac{1}{C}, \tag{4}$$

where F_2 is a focal length of the achromat lens and is set to F_2 = 100 mm. Distance B is found to be 951.89 mm. Substituting these parameters into Eq. (4), we calculate distance C as C = 111.74 mm.

For an achromatic imaging system to be achieved, it is required that Eq. (1) be satisfied. The wavelength dependence of the power of the projection lens, $\varphi_1(\lambda)$, is shown in Fig. 9. The h-line projection lens is designed to be least sensitive to the wavelength variations around the h line (λ = 405.5 nm). The

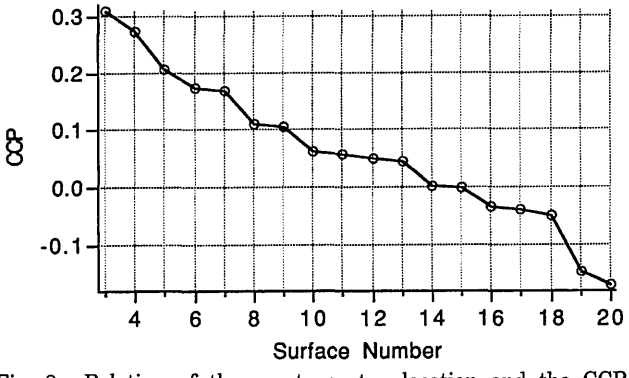

Fig. 8. Relation of the aperture stop location and the CCP. When the stop is set 1.9 mm behind surface 14, the CCP becomes exactly zero.

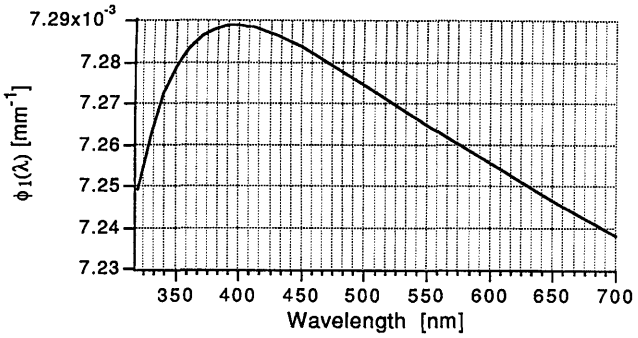

Fig. 9. Wavelength dependence of the power of the h-line projection lens, $\varphi_1(\lambda)$.

spectral range of the light (550–650 nm) used for the alignment system is far enough from the h line to produce an approximately linear dependence of lens power, $\varphi_1(\lambda)$, versus wavelength, λ. In Eq. (1), $\varphi_3(\lambda_0)$ is set to $1/55$ mm^{-1} so that the total magnification of the system will be approximately 5/1. By substituting the above parameters into Eq. (1), we obtain the required power for lens 3, $\varphi_3(\lambda)$. Figure 10 shows a plot of the required lens power, $\varphi_3(\lambda)$. Note that $\varphi_3(\lambda)$ is also approximately linear because of the linearity of $\varphi_1(\lambda)$ in the wavelength range between 550 and 650 nm. The following solution is based on this linearity of optical powers with wavelength. However, it is important to emphasize that this solution is also applicable to projection lenses designed for operation with an i-line (λ = 365 nm) exposure wavelength or the excimer laser (λ = 248 nm) illumination, because these lenses are also optimized at the exposure wavelength and their relations between the power and the wavelength are also approximately linear in the range of visible light used for the alignment system.

To obtain the best fit to the theoretical curve shown in Fig. 10, we employ a refractive–diffractive hybrid lens. The hybrid lens in Fig. 4 consists of a refractive doublet and a diffractive lens element. Using thin-lens theory, we find that the total power of the hybrid lens is given by

$$\varphi_3(\lambda) = \varphi_{rA}(\lambda) + \varphi_{rB}(\lambda) + \varphi_d(\lambda), \tag{5}$$

where φ_{rA} is the power of the first part of the refractive doublet, φ_{rB} is the power of the second part

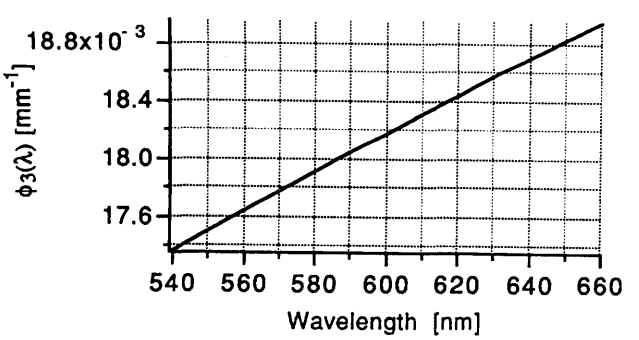

Fig. 10. Required lens power, $\varphi_3(\lambda)$, for an achromatic system.

of the refractive doublet, and φ_d is the power of the diffractive lens. The first derivative of Eq. (5) is given by

$$\Delta\varphi_3 = -\left[\frac{\varphi_{rA}(\lambda_0)}{V_{rA}} + \frac{\varphi_{rB}(\lambda_0)}{V_{rB}}\right] + \varphi_d(\lambda_0)\frac{\Delta\lambda}{\lambda_0}, \tag{6}$$

in which

$$V_{rA} = \frac{n_{rA}(\lambda_0) - 1}{n_{rA}(\lambda_2) - n_{rA}(\lambda_1)},$$

$$V_{rB} = \frac{n_{rB}(\lambda_0) - 1}{n_{rB}(\lambda_2) - n_{rB}(\lambda_1)},$$

where λ_0 = 600 nm, λ_1 = 550 nm, λ_2 = 650 nm, and $\Delta\lambda$ = 100 nm.

To obtain the best fit to the theoretical curve shown in Fig. 10, we find that the following condition is required:

$$\frac{\varphi_{rA}(\lambda_0)}{V_{rA}} + \frac{\varphi_{rB}(\lambda_0)}{V_{rB}} = 0; \tag{7}$$

this is the condition required if the refractive doublet is to be an achromat. Using Eqs. (6) and (7), we find the required power of the diffractive lens to be

$$\varphi_d(\lambda_0) = \frac{\lambda_0}{\Delta\lambda}\Delta\varphi_3, \tag{8}$$

and the total power of the doublet is

$$\varphi_{rA}(\lambda_0) + \varphi_{rB}(\lambda_0) = \varphi_3(\lambda_0) - \varphi_d(\lambda_0). \tag{9}$$

The required powers for each component of the doublet are obtained through the use of Eqs. (7) and (9) as follows:

$$\varphi_{rA} = \frac{V_{rA}}{V_{rA} - V_{rB}}[\varphi_3(\lambda_0) - \varphi_d(\lambda_0)], \tag{10}$$

$$\varphi_{rB} = \frac{V_{rB}}{V_{rB} - V_{rA}}[\varphi_3(\lambda_0) - \varphi_d(\lambda_0)]. \tag{11}$$

Alternatively, these powers can be described in terms of surface curvatures:

$$\varphi_{rA}(\lambda_0) = [n_{rA}(\lambda_0) - 1](c_2 - c_1) \tag{12}$$

$$\varphi_{rB}(\lambda_0) = [n_{rB}(\lambda_0) - 1](c_3 - c_2), \tag{13}$$

where c_1 and c_2 are the curvatures of the front and the rear surface of the first part of the doublet, respectively and c_3 is a curvature of the rear surface of the latter part of the doublet. To simplify the fabrication of the diffractive lens on the rear surface of the doublet, we set curvature c_3 to zero (i.e., it is required to be a flat surface). Once we calculate $\varphi_d(\lambda_0)$ by using Eq. (8), we obtain c_2 by using Eqs. (11) and (13); we calculate c_1 by using Eqs. (10) and (12). For this design example, we choose the following glass types for the doublet: Schott BK7 and F2, which are

inexpensive glass types commonly used in industry. Using the design methodology described above, we obtain the first-order design parameters for the hybrid lens: $\varphi_d(\lambda_0) = 0.0075\ \text{mm}^{-1}$, $c_1 = 0.0255\ \text{mm}^{-1}$, $c_2 = -0.0241\ \text{mm}^{-1}$, and $c_3 = 0$. These parameters and distance C are then optimized through the utilization of commercial lens-design software. Table 1 shows the lens data obtained after optimization.

For optimization with commercial lens-design programs, it is convenient to describe the diffractive lens in the same manner as a refractive lens. Sweatt proposed a convenient method to describe a diffractive lens for use with lens-design software in his paper.[10] With this method, the power of a diffractive lens, $\varphi_d(\lambda)$, can be described as a thin lens that possesses a very large index of refraction, i.e.,

$$\varphi_d(\lambda) = [n(\lambda) - 1](c_A - c_B), \tag{14}$$

Table 1. Lens Data for the Achromatic Alignment System[a]

Surface	Curvature (mm^{-1})	Thickness (mm)	Glass
Object	0.00000000	12.836980	Air
S1	0.00920404	3.810000	Schott LF5
S2	0.01812579	30.649824	Air
S3	−0.02523014	6.350000	Fused silica
S4	−0.01903636	12.037365	Air
S5	−0.00902611	13.390880	Fused silica
S6	−0.01236653	4.795520	Air
S7	0.00285564	31.750000	Fused silica
S8	−0.01021591	2.540000	Air
S9	0.00531074	35.560000	Fused silica
S10	−0.00915616	1.893291	Air
S11	−0.00964527	8.321446	Schott LF5
S12	0.00775857	1.783080	Air
S13	0.00762794	40.640000	Fused silica
S14	−0.00574017	2.540000	Air
S15	0.00872893	31.750000	Fused silica
S16	−0.00162331	2.540000	Air
S17	0.01518926	7.620000	Fused silica
S18	0.01815358	48.874223	Air
S19	−0.01119420	7.620000	Schott LF5
S20	0.00558275	3.540000	Air
S21	0.00000000	15.151860	Air
S22	−0.02072136	21.414740	Fused silicia
S23	−0.01501763	3.169920	Air
S24	−0.00302574	17.780000	Fused silica
S25	−0.00817112	2.540000	Air
S26	0.00079734	15.240000	Fused silica
S27	−0.00336819	0.000000	
S28	0.00331052	15.240000	Fused silica
S29	0.00042021	622.440000	Air
S30	0.01555694	6.230000	Schott SK11
S31	−0.02223210	2.500000	Schott SF5
S32	−0.00554232	100.473524	Air
Stop	0.03318571	5.300000	Schott BK7
S34	−0.04330520	4.000000	Schott F2
S35	0.00000000	0.000100	Virtual
S36	−0.00000063	103.095781	Air
Image	0.00000000	0.000000	

[a]The broadband (500–650 nm) alignment system design has a magnification of 5×, a N.A. of 0.175, and an object height of 10 mm.

in which

$$n(\lambda) = \frac{\lambda}{\lambda_0} N + 1, \tag{15}$$

where c_A and c_B are the curvatures of a diffractive lens and $n(\lambda)$ is an effective refractive index of the diffractive lens. To model the behavior of a diffractive lens accurately, N should be a very large number. In practice, N is typically set to $N = 10{,}000$. Using this method, one can describe a diffractive lens just like a refractive lens. The curvature, c_A, which corresponds to the curvature of the rear surface of the doublet in the hybrid lens, is set to zero for ease of fabrication.

Figure 11(a) shows a plot of the difference in image plane location, ΔL, at wavelength λ, relative to the location of the image plane at the center wavelength ($\lambda_0 = 600$ nm), and Fig. 11(b) shows the relationship of the image magnification difference, ΔM, at different wavelengths, respectively. Note that in the region from 550 to 650 nm, the spread of ΔL is less than 50 μm and the spread of ΔM is less than 0.05%. Originally, without the correction system (see Fig. 5), these numbers were 11.28 mm and 1.18%, respectively.

4. Design and Fabrication of the Diffractive Lenses

Once a value for $\varphi_d(\lambda_0)$ is obtained, a blaze profile of a diffractive lens surface, $d(r)$, can be calculated as

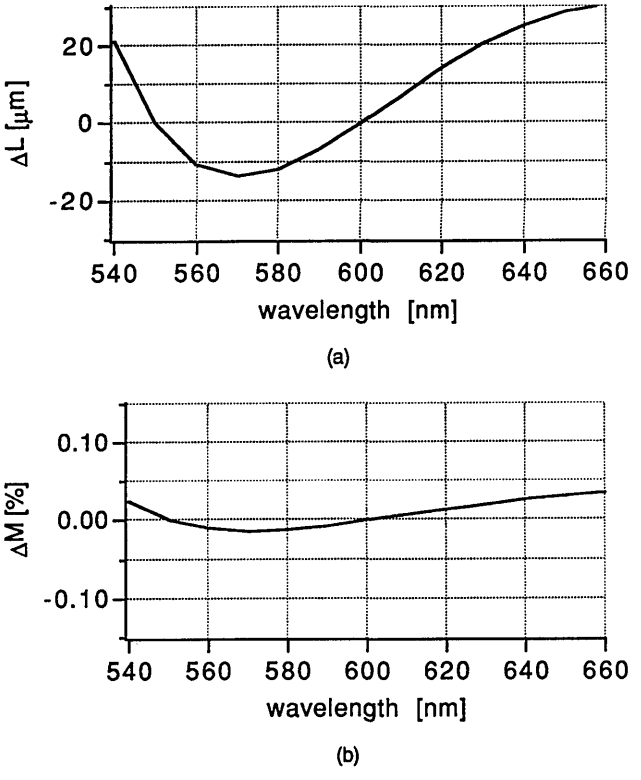

Fig. 11. Chromatic image differences with the chromatic aberration correction system. It is found that peak-to-peak values of (a) ΔL and (b) ΔM in the wavelength range between 550 and 650 nm are 50 μm and 0.05%, respectively.

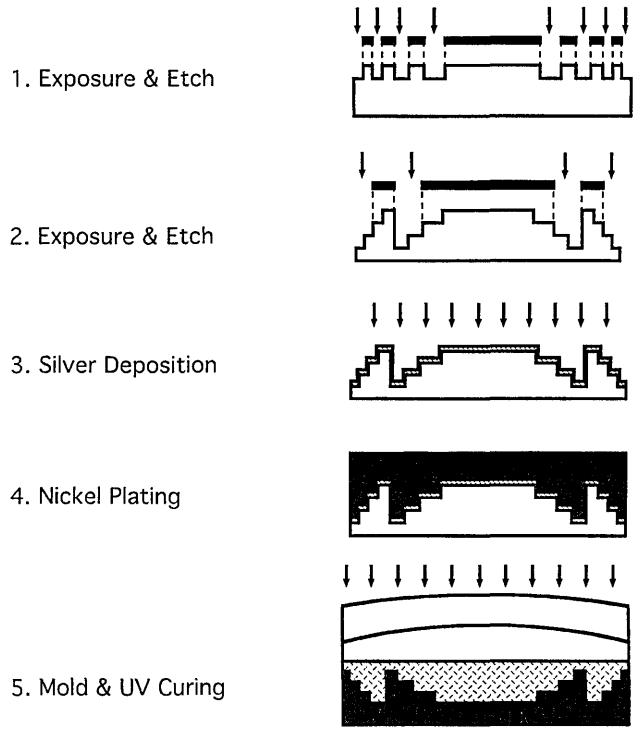

Fig. 12. Fabrication process of a four-step diffractive lens. The processing steps are discussed in detail in the text.

follows:

$$d(r_m) = d_{\max}\left[m - \frac{\varphi_d(\lambda_0)}{2\lambda_0} r_m^2\right], \tag{16}$$

in which

$$d_{\max} = \frac{\lambda_0}{n_{\text{dif}} - 1}, \quad \left[\frac{2(m-1)\lambda_0}{\varphi_d(\lambda_0)}\right]^{1/2} \le r_m < \left[\frac{2m\lambda_0}{\varphi_d(\lambda_0)}\right]^{1/2}, \tag{17}$$

where m is an integer > 0, r_m is the coordinate in the radial direction, and n_{dif} is a refractive index of an actual material of the diffractive lens. Equation (16) gives a parabolic profile. We approximated this profile by using four phase steps. Figure 12 illustrates the fabrication process for a four-step diffractive lens. In steps 1 and 2, a four-step silicon master is fabricated through the use of a photolithographic lithographic process. So that a conductive surface is obtained, silver is deposited in step 3. Then, through the use of electroplating, a nickel (negative) stamper is formed on the silicon master in step 4. Step 5 illustrates the molding process. We used UV curing cement to mold the four-step diffractive lens on the flat surface of a doublet glass lens. After UV curing, the nickel stamper is separated from the hybrid lens. Figure 13 shows scanning electron microscope photographs of the silicon master and the nickel stamper. In the present design, the maximum depth is 0.8 μm and the minimum zone width at the edge of the lens is approximately 3 μm.

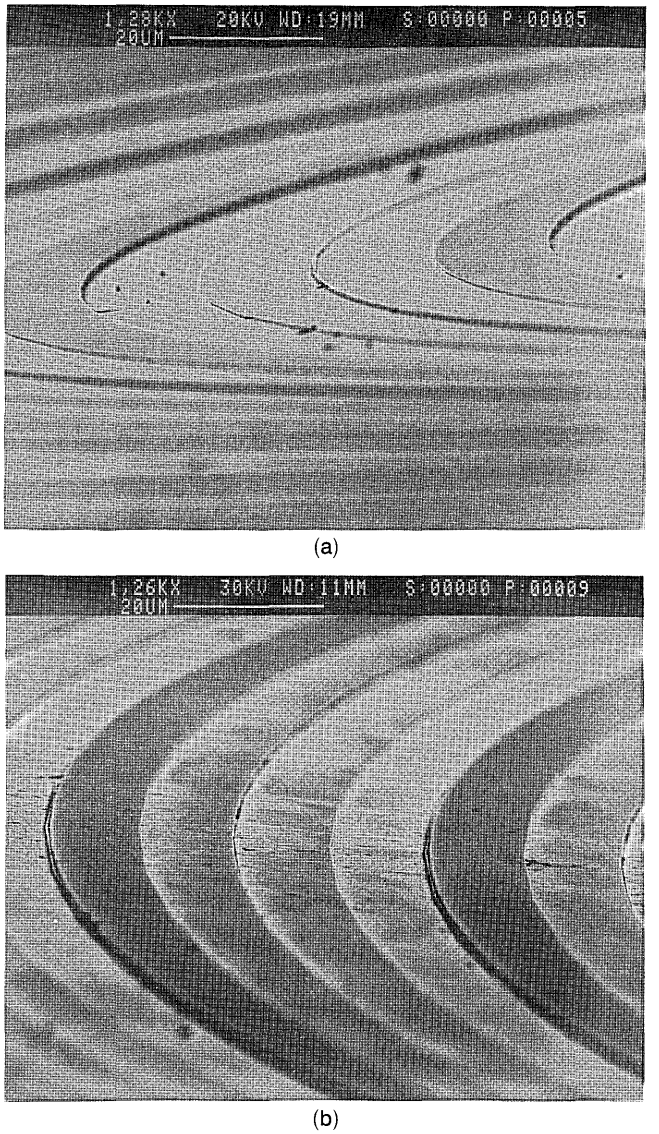

Fig. 13. Scanning electron microscope photographs of (a) the silicon master and (b) the nickel stamper.

5. Experimental Results

Figure 14 illustrates an experimental setup for the evaluation of the paraxial performance of our correction system. We used a triplet lens as a substitute for the projection lens. With the illumination of the center wavelength (600 nm), the first image of

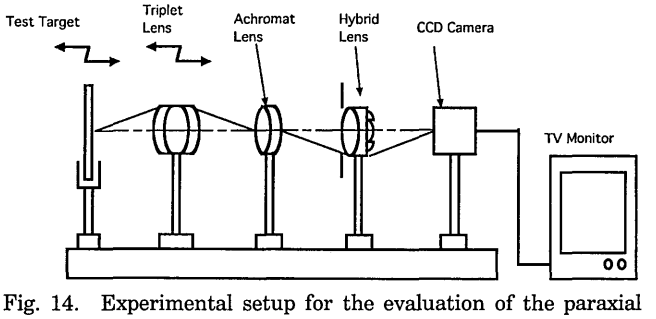

Fig. 14. Experimental setup for the evaluation of the paraxial performance of the correction system.

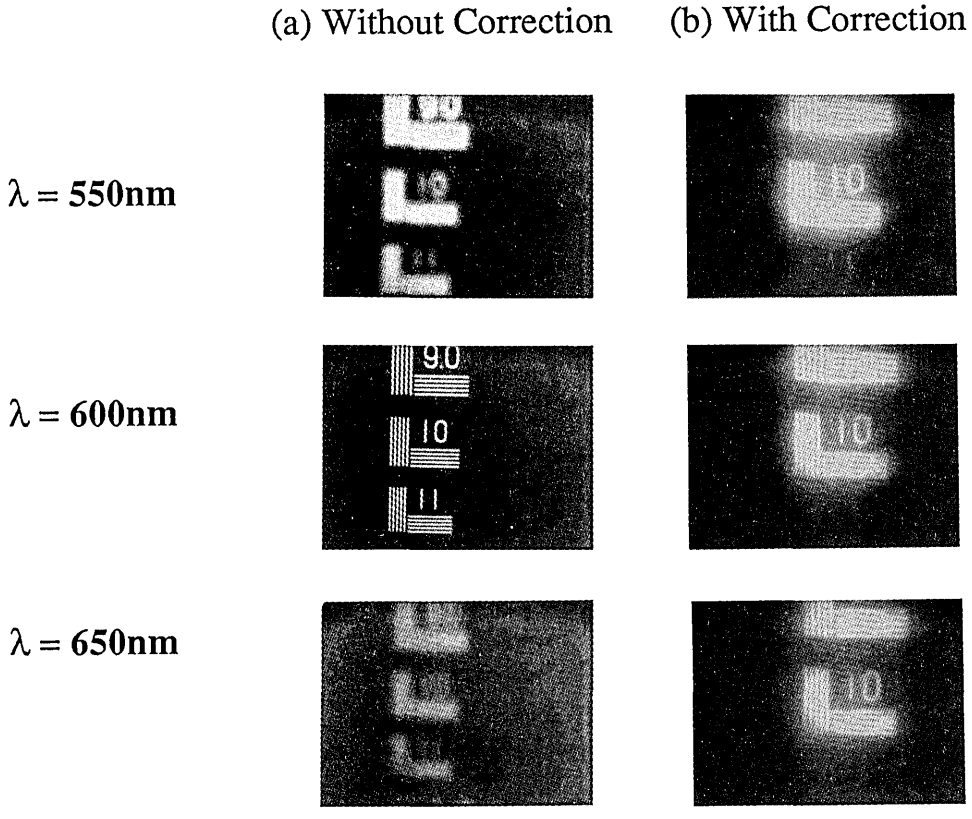

Fig. 15. Photographs of images of the test targets, showing (a) the first images formed by the triplet lens (i.e., without the correction system), (b) the secondary images of the test targets formed by the correction system. Numbers in the pictures indicate the numbers of lines/1 mm.

the test target is formed at the front principal point of the achromat lens. As a way to simulate the longitudinal chromatic aberration of the projection lens, the test target and the triplet lens are moved by the amount corresponding to ΔL at the wavelengths of 550 and 650 nm in Fig. 5(a), respectively. Relative locations of the first images formed by the triplet lens coincide with those of the projection lens. Although any high-order aberrations are different from those of the projection lens, paraxial longitudinal chromatic aberration can be corrected in this setup. Figure 15(b) shows secondary images of the test targets formed by the correction system. For comparison, the first images formed by the triplet lens (i.e., without the correction system) are shown in Fig. 15(a). Without the correction system, images at 550 and 650 nm are severely degraded because they are out of focus. However, with the correction system, the differences of the first image points are well corrected at the secondary image plane on the CCD camera. It should be noted that degradation of the image with the correction system is mainly due to the difference of the higher-order aberrations between the experimental setup and the real projection lens. In Fig. 15(b), flare light can be seen in the background. The flare light is associated with undiffracted light light-diffracted higher diffraction orders. One can reduce the flare light significantly by increasing the number of steps in the structure, i.e., by improving the diffraction efficiency of the diffractive lens.

6. Conclusion

We have proposed a broadband alignment scheme for a stepper system that uses a refractive–diffractive hybrid lens. The hybrid lens consists of a refractive achromatic doublet and a diffractive lens. A diffractive lens generates a linear dependence of lens power versus wavelength, which matches a characteristic of the h-line projection lens in the visible light region. A refractive achromatic doublet controls the total power. To correct a lateral chromatic aberration, we set an aperture stop in contact with the hybrid lens. With the proposed system, the spread of image planes and magnification difference in the spectral range from 550 to 650 nm can be reduced to 50 μm and 0.05%, whereas without the correction system these values are 11.28 mm and 1.18%, respectively.

A photolithographic process and electroplating method were used to fabricate a surface-relief master with which diffractive lenses were molded with UV cement. The experimental results show good image correction over the 550–650-nm wavelength band. It is noted that this design methodology is also applicable to i-line and excimer laser stepper systems, or to any other monochromatic lenses that have a linear dependence of lens power versus wavelength.

The authors are grateful to D. Faklis at Rochester Photonics Corporation for his helpful discussions on fabrication of diffractive lenses, D. Lilienfeld at the Cornell National Nanofabrication Facility for fabricating the diffractive lens master, and B. McIntyre and M. Missig at the University of Rochester for their assistance in evaluating the diffractive lens.

References

1. K. Ota, N. Magome, and K. Nishi, "New alignment sensors for wafer stepper," in *Optical/Laser Microlithography IV,* V. Pol, ed., Proc. Soc. Photo-Opt. Instrum. Eng. **1463,** 304–314 (1991).
2. K. Nishi, "Alignment system for exposure apparatus," U.S. patent 4,962,318 (9 October 1990).
3. S. Komoriya, T. Kawanabe, S. Nakagawa, T. Oosakaya, and N. Iriki, "Method of making semiconductor integrated circuit, pattern detecting method, and system for semiconductor alignment and reduced stepping exposure for use in same," U.S. patent 5,094,539 (10 March 1992).
4. T. Sone and N. George, "Hybrid diffractive-refractive lenses and achromats," Appl. Opt. **27,** 2960–2971 (1988).
5. D. R. Shafer, "Lens usable in the ultraviolet," U.S. patent 4,770,477 (13 September 1988).
6. M. Born and E. Wolf, *Principles of Optics* (Pergamon, Bristol, 1974), pp. 64–93.
7. A. Offner, "Field lenses and secondary axial aberration," Appl. Opt. **8,** 1735–1736 (1969).
8. D. Faklis and G. M. Morris, "Broadband imaging with holographic lenses," Opt. Eng. **28,** 592–598 (1989).
9. W. T. Welford, *Aberrations of Optical Systems* (Hilger, Bristol, 1989), p. 207.
10. W. C. Sweatt, "Describing holographic optical elements as lenses," J. Opt. Soc. Am. **67,** 803–808 (1977).